Experimental study of an adiabatic two-phase flow in a simulated PWR spent fuel bundle

Guillaume Brillant, Jimmy Martin, Benjamin Fourré

EXPERIMENTAL STUDY OF AN ADIABATIC TWO-PHASE FLOW IN A SIMULATED PWR SPENT FUEL BUNDLE

G. Brillant, J. Martin, and B. Fourré
Institut de Radioprotection et de Sûreté nucléaire (IRSN),
Nuclear Safety Division,
Safety Research, Cadarache, St Paul-Lez-Durance 13115, France
Guillaume.Brillant@irsn.fr, Jimmy.Martin@irsn.fr, Benjamin.Fourre@irsn.fr

ABSTRACT

Within the framework of the post-Fukushima actions, an experimental project named DENOPI has been launched with the aim to study the behavior of spent fuel pools under loss of cooling and loss of coolant conditions. Within this project, the MEDEA facility is intended to study the thermalhydraulics of a fully covered or uncovered spent fuel bundle. It consists in a hydraulic loop connected to an experimental test section in which a simulated one meter high PWR spent fuel bundle is located. The MEDEA-overflow experiments, presented in this study, consist in adiabatic air/water flows in a fully covered unheated bundle. Axial pressure and void fraction distributions were measured using pressure transducers. Overall, the tests exhibited two different flow regimes. Indeed, at low gas superficial velocities, a bubbly flow set up within the bundle whereas a transition to slug flow was obtained at larger ones.

KEYWORDS
Spent Fuel Pool, loss-of-cooling/loss-of-coolant accident, DENOPI project, Two-phase flow

1. INTRODUCTION

The vulnerability of Spent Fuel Pools (SFP) has been replaced to the front of the stage since the Fukushima-Daiichi accident [1–4] and several kinds of actions have been launched in order to understand and reduce the risk and consequences of potential accidents on SFP. For instance, a working group set up at OECD/NEA issued a status report on SFP Loss-of-Cooling and Loss-of-Coolant Accident (SFP-LOCA), that aims at providing a summary of the status of SFP accident and mitigation strategies, a brief review of the state of the art of the simulation tools potentialities for SFP-LOCA assessment and a proposal for some additional research actions [5]. Moreover, a European NUGENIA project named Air-SFP was performed in 2015-2016, in order to assess the uncertainties of Severe Accident (SA) codes in dealing with SFP-LOCA and to identify needs of modeling improvement [6]. Recently, a Phenomena Identification Ranking Table (PIRT) activity related to SFP-LOCA was carried out at OECD/NEA [7]. From these activities, it appears that the validation database of most computer codes currently used for SFP deterministic safety analysis (system codes developed on the basis of in-reactor incidental or accidental conditions) needs to be extended to SFP configurations. Indeed, the thermal-hydraulics of a SFP is mainly based on natural convection flows (gaseous, liquid or two-phase flows), developed at atmospheric pressure with a relatively low heat load, compared to in-reactor conditions. These current

codes haven’t been primarily developed for natural convection flows and their applicability to SFP has to be improved.

In this context, the DENOPI project [8–10] has been launched by the IRSN (the French Technical and Scientific Support Organization) in collaboration with several research laboratories with the aim of studying the behavior of spent fuel pools under Loss-of-Cooling and Loss-of-Coolant Accidents (SFP-LOCA). The DENOPI project is a research program including both experimental and modeling activities. Its purpose is to provide code developers with an experimental database, made up of SFP integral and separate effect tests, for code improvement and validation. The project is divided into three axes, each corresponding to a specific spatial scale involved in a SFP-LOCA. The first axis is related to the two-phase natural convection flows occurring at the pool scale, prior to the fuel uncovery. The thermal-hydraulics of a typical PWR (Pressurized Water Reactor) fuel bundle prior and after the fuel uncovery is investigated in the second axis. In particular, the efficiency of spray cooling systems as a mitigation measure is assessed. Finally, the third axis is dedicated to the fuel cladding degradation by steam-air mixture oxidation after fuel uncovery.

The MEDEA mock-up was built within the framework of the DENOPI project, and more specifically in its second axis. The main component of this facility is a one meter high unheated rod bundle. The objective of this experimental set-up is to get new insights on the physical phenomena involved during uncovering and water spraying of a fuel bundle stored in a spent fuel pool. The MEDEA program has two main steps. The first one is focused on air/water experiments, and the second one on steam/water experiments. The air/water experiments are of two kinds: the study of flooding in case of water spraying on a completely uncovered bundle (MEDEA-flooding tests) and the study of the void distribution along a fully covered assembly in an air/water co-current flow (MEDEA-overflow tests). The results of the MEDEA-overflow tests are presented in this article. The MEDEA-overflow tests aim at studying the pressure loss and void fraction along a PWR fuel bundle for a co-current air/water flow at room temperature and atmospheric pressure. These measurements are required for the validation of thermal-hydraulics numerical tools, especially regarding the drift flux models for the low pressure domain of natural flow in a fuel bundle. This air/water flow study is a first approach to observe and measure the flow pattern and void fraction for a co-current gas/liquid flow awaiting the ASPIC facility. Actually, the ASPIC facility, currently under construction, is a full height 17x17 assembly with heated rods (80kW, up to 600 °C) that will enable several kinds of experiments and scenarios for SFP accidents at the assembly scale.

This article is organized as follows. In section 2, a presentation of the MEDEA device and measurement apparatus is driven. The test parameters and the experimental protocol are laid out in section 3. Then, the results of the test series are stated and analyzed in section 4. Finally, the main outcomes of this experimental study are drawn in the conclusion.

2. DESCRIPTION OF THE OVERFLOW CONFIGURATION OF THE MEDEA FACILITY

Several experimental rigs are planned in the framework of the DENOPI project. The MIDI facility [9, 11] will be devoted to the investigations on large scale flow patterns and onset of boiling in SFP before the dewatering of the fuel bundles. The MEDEA and ASPIC test rigs are dedicated to the study of the physical phenomena involved at the assembly scale during a SFP deflooding. All these new facilities will belong to the IRSN platform THEMA (THErmalhydraulics for Mitigation of Accidents). The overflow configuration of the MEDEA facility is composed of a test section with a one meter high rod bundle, an air injection line connected to the bottom of the test section, a water injection line connected to the bottom of the test section, and a water gathering circuit for the overflow liquid (Cf. figure 1).

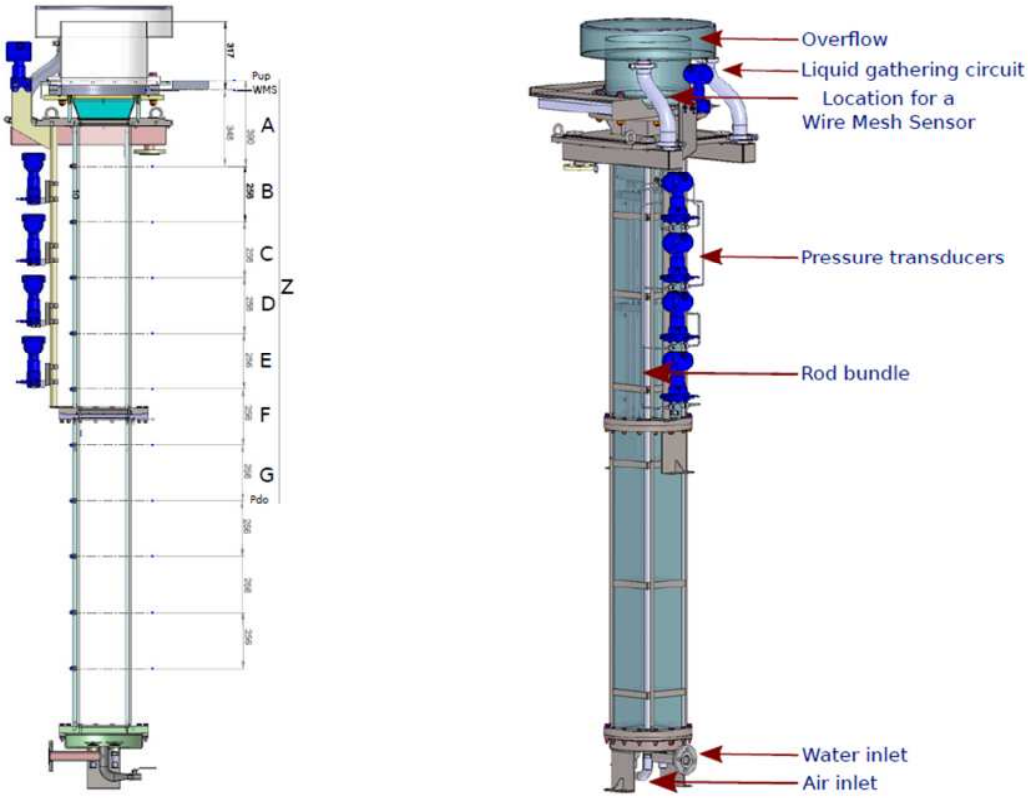

Figure 1. Locations of the pressure measuring holes (A to G) on the MEDEA-overflow test section.

The MEDEA assembly consists in a 17x17 rod bundle with a reduced height of 1240 mm for a weight of about 80 kg. The rods have an outer diameter of 9.5 mm and the pitch of the assembly is 12.6 mm. The 25 guide tubes of the bundle have an outer diameter of 12 mm. The three grids of the bundle consist in a mixing grid in between two support grids. There is 530 mm between the upper support grid and the mixing grid and 400 mm between the mixing grid and the lower support grid. The central test section, in which the assembly is inserted, is a square tube with an internal dimension of 225 mm corresponding to a cell of a spent fuel pool rack. The top nozzle, spacer grids, and rods used to build the assembly are representative to a typical PWR rod bundle. The free flow area of the top nozzle is about 205 cm^2. Below the test section with the rod bundle, the lower section aims at injecting the water flow and the air bubbles and obtaining a stationary flow at the bottom of the rod bundle. The length of the lower section is 1416 mm (about 6 hydraulic diameters). Above the test section, the upper head is connected to the gathering water line that collects the overflow. Note that about 317 mm below the overflow level could be placed a Wire Mesh Sensor (WMS) [12, 13] which provides measurements of the void fraction on a grid pattern. These measurements are under analysis and will be presented and discussed in a forthcoming article.

In order to regulate the air volume flowrate injected in the test section, a flowmeter/valve group is incorporated in the air injection line. This flowmeter/valve group is used in automatic mode. That way, the operator sets the target flowrate which is stabilized by means of a PID controller. The water injection line is connected to a tank with a capacity of 2000 l. The water is pumped from that tank and flows through a flowmeter/valve group. This group can either be used in manual or automatic mode to set up the water mass flowrate in injection line. The water flows through the central section and the rod bundle.

Note that a bypass line can be partially opened with manual valve to send back part of the water flow directly to the main tank. The water flow above the rod bundle leads to an overflow that is collected and sent back by gravity to the main tank by means of the water gathering line.

3. TEST PARAMETERS AND EXPERIMENTAL PROTOCOL

The MEDEA-overflow test series has three main parameters: the water mass flowrate, the air volume flowrate and the geometrical configuration. Two configurations have been considered: with (configuration C1) and without (configuration C2) the rod bundle inside the central test section. That way, the impact of the rod bundle on the evolution of the pressure loss and void fraction all along the test section can be directly evaluated. The range of the water mass flowrate is 400 g/s to 2400 g/s and the range of the air flowrate is 10 Nl/min to 180 Nl/min (flowrate at 0 °C and 1 atm).

The experimental protocol of the MEDEA-overflow tests is based on the variation of the air flowrate injection while the water mass flowrate and the geometrical configuration are unchanged. Actually, the series started with a test at zero air flowrate to determine the default signal of all the pressure transducers. That way, the transducers inherent offset (*e.g.* due to transducer orientation) as well as the potential dynamic pressure offset can be subtracted from the other tests with positive gas flowrates. Note that the free flow section is not constant along the test section which leads to variations of the water velocity and thus of the dynamic pressure. For each test, the signal of the pressure transducers is recorded over at least 10 min at 1 Hz. Hence, stabilized mean and standard deviation values of the pressures can be calculated. The locations of all the pressure transducers are reported in figure 1. The uncertainties of the pressure measurements, considering both the sensor and the supply chain, are 0.05 mbar for the differential pressure transducers dP_A-dP_G and 1.5 mbar for the absolute pressure transducers P_{up} and P_{do}. As far as the flowrate measurements are concerned, the uncertainties are 1 % for the air flow and 0.1 % for the water flow. Regarding the absolute pressure measurements, the pressure difference $P_{do}-P_{up}$ can be written as (terms with air density are neglected as well as the dynamic pressure drop between two sensors):

$$dP_Z = P_{do} - P_{up} = (1-\alpha_Z)\cdot\rho_w\cdot g\cdot h + \rho_w\cdot g\cdot(H-h) \tag{1}$$

Where H is the elevation difference between the two transducers, h the elevation difference between the two connection holes on the central section, and α_Z the mean void fraction along the test section between the two holes where the two transducers P_{up} and P_{do} are connected. Therefore, the void fraction α_Z can be estimated as:

$$\alpha_Z = \frac{(\rho_w\cdot g\cdot H - dP_Z)}{\rho_w\cdot g\cdot h} \tag{2}$$

Concerning the differential pressure measurements, the following expression can be written:

$$dP_i - dP_i^0 = \rho_w\cdot g\cdot dh_i - (1-\alpha_i)\cdot\rho_w\cdot g\cdot dh_i \quad ; \quad i = A,\dots,G \tag{3}$$

with dP_i^0 the offset signal of the differential pressure transducers and dh the elevation difference between the two connections of the dedicated transducer. Therefore, the void fraction can be calculated as:

$$\alpha_i = \frac{(dP_i - dP_i^0)}{\rho_w\cdot g\cdot dh_i} \quad ; \quad i = A,\dots,G \tag{4}$$

The void fractions profiles presented hereafter were calculated by means of these expressions.

4. RESULTS

4.1. Pressure measurements for the series at a water flowrate of 1200 g/s

For this test series, eleven values of the air volume flowrate are considered in the range 0 Nl/min to 180 Nl/min and the water mass flowrate is kept constant to the value of 1200 g/s during each test (meaning each plateau of air flowrate). As the friction inside the test section evolves with the air flowrate, the opening rate of the valve on the water line was adapted on each test to stick to the target value of the water mass flowrate. In doing so, the mean value of the water mass flowrate is kept in the range 1198 g/s to 1223 g/s (2 % maximum deviation). It can be noticed that, for all tests, the standard deviation of the water mass flowrate is around 1.5 g/s.

The mean value of the pressure difference $P_{do} - P_{up}$ on the test section is given in figure 2a. This pressure difference decreases from 196.0 mbar to 165.9 mbar while the air flowrate rises from 0 Nl/min to 180 Nl/min. The measurements from the differential pressure transducers, gathered in figure 2b, reveal a variation in the range 0 mbar to 6 mbar. Concerning the standard deviation of the pressure signals (Cf. figure 3), it can be noticed that the standard deviation of the differential pressure transducers clearly increases with the air volume flowrate. However, this trend cannot be observed in figure 3a for the absolute pressure measurement on the full height of the section. This can probably be imputed to the higher uncertainty of the absolute pressure transducers. Besides, it can be noted that the standard deviation above the rod bundle (curve A, figure 3b) is higher than the standard deviation in the assembly area, revealing a more perturbed flow in this region.

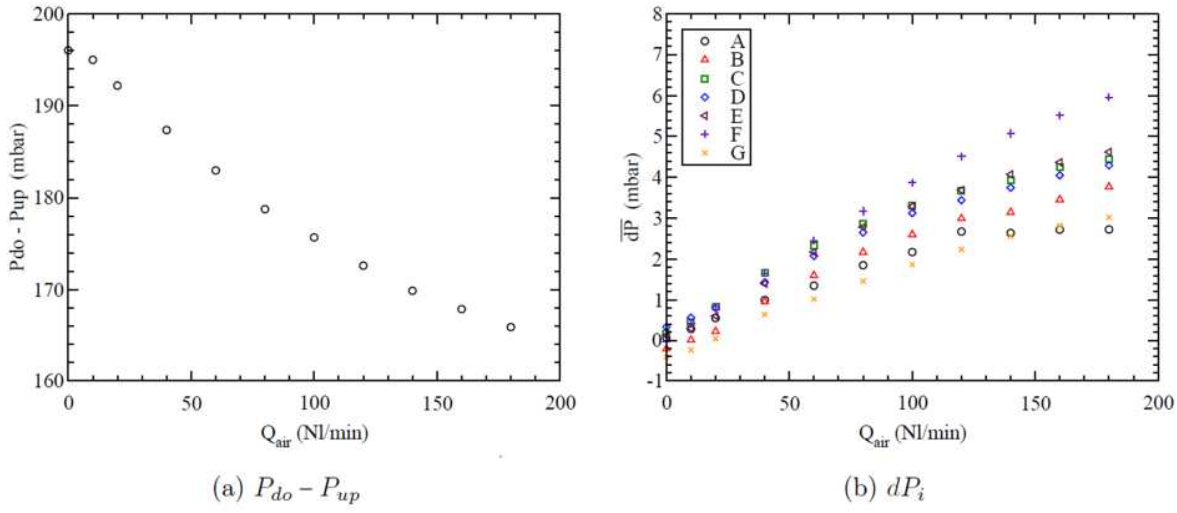

Figure 2. Mean pressure measurements for the tests at a water flowrate of 1200 g/s.

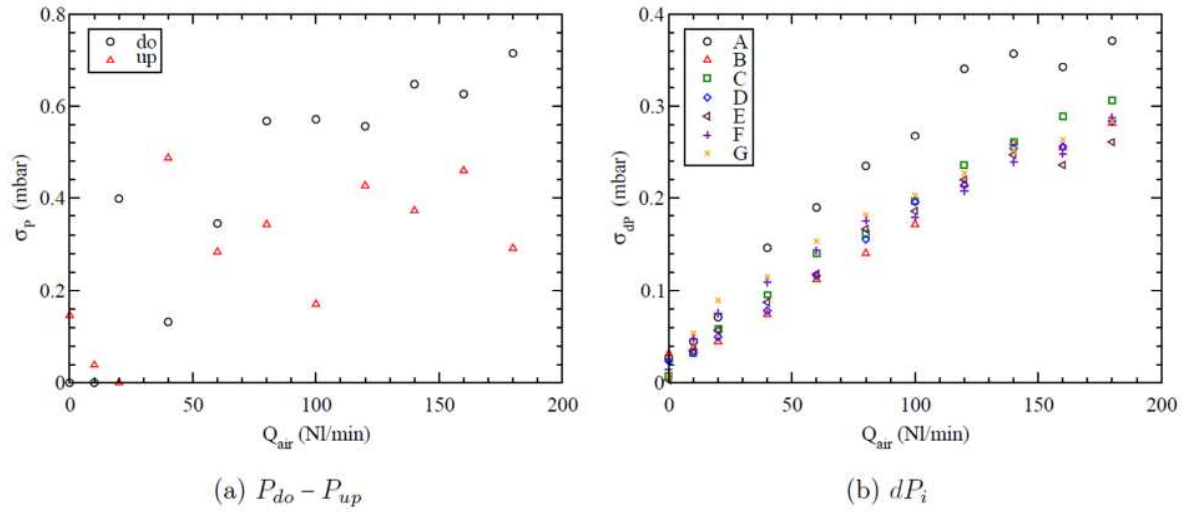

(a) $P_{do} - P_{up}$ (b) dP_i

Figure 3. Standard deviation of the pressure measurements for the tests at a water flowrate of 1200 g/s.

4.2. Void fraction with/without assembly at Q_w = 1200 g/s

The void fractions, calculated by means of the pressure measurements and equations (2) and (4), are plotted in figure 4a for the test series with the rod bundle inserted into the test section. Firstly, the lower values of the void fraction are measured above the rod bundle (transducer A). In fact, these smaller values may be ascribed to the higher section radius above the assembly and to the recirculations observed below the overflow water level. It can be noticed a stabilization at this location of the void fraction around 7 % for the air volume flowrates higher than 120 Nl/min. The highest values of the void fraction are measured just below the rod bundle (transducer F) and are due to a plug created by the lower plate below the assembly. Note that this plug grows, as well as the void fraction, as the air volume flowrate rises. Intermediary void fraction are observed all along the rod bundle (transducers B-E) as well as in the lower part of the test section (transducer G). The impact of the grids on the void fraction profiles can be hardly explained. In fact, the transducers B (with a support grid) and D (with a mixing grid) lead to similar void fraction profiles but a different behavior is noted for the transducer E (with a support grid). The void fraction in the lower part of the test section (transducer G) is lower than the void fraction along the rod bundle. This observation can be imputed to the higher friction in the assembly (due to both rods and grids). The mean void fraction (α_Z) over the full height of the test section measured by the two absolute pressure transducers is among the other void fraction curves measured locally by all the differential pressure transducers.

This test series was repeated without the rod bundle in the central test section in order to give information for the code development and validation. The void fraction measured during the test series without the assembly in the central test section are reported on figure 4b as a function of the air volume flowrate. It can be noticed that the measurements for the transducers B to E are quite clustered due to the absence of the assembly. The void fraction differences between the tests with and without the subassembly in the central section are given on figure 5. The differences of void fraction between with and without bundles tests increase with the air volume flowrate. It is consistent with the fact that the fluid frictions rises with the velocity and hence with the flowrates. However, the differences remain below 5 % for the range of value of the air and water flowrates. It can be observed that the larger differences are observed for the transducers B to E which corresponds to the area of the rod bundle.

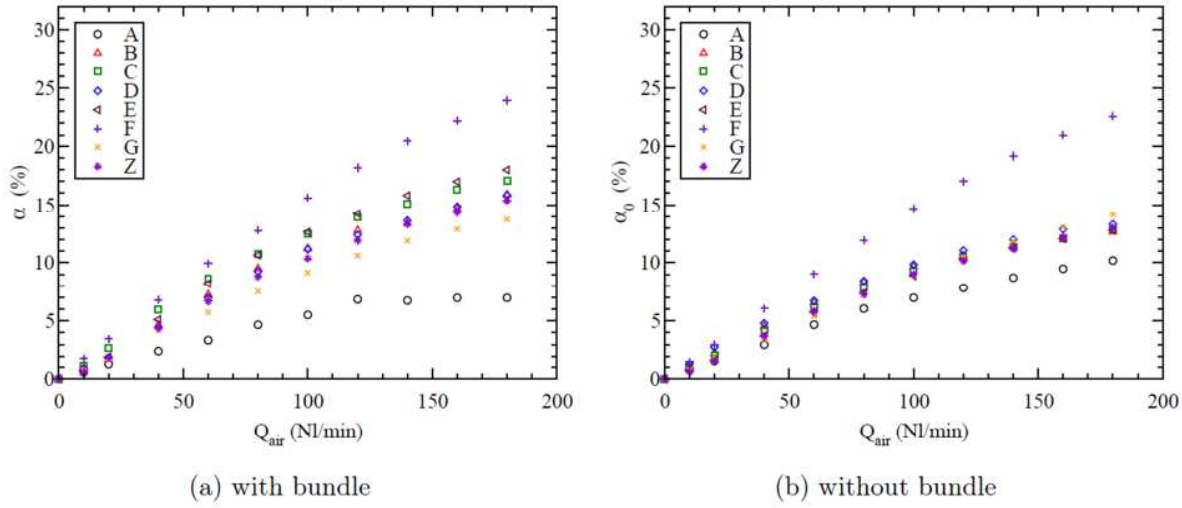

Figure 4. Void fraction for the tests at a water mass flowrate of 1200 g/s.

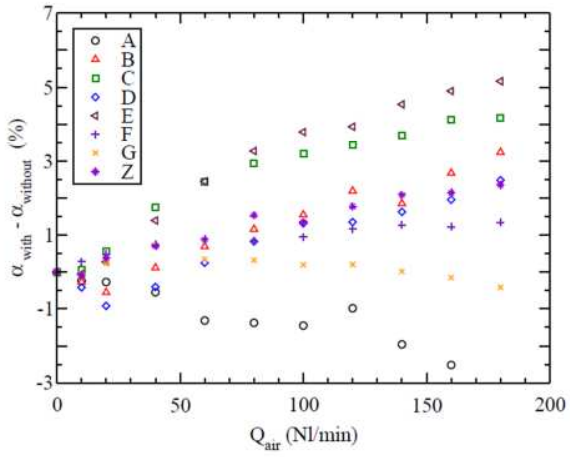

Figure 5. Void fraction difference for the tests with/without assembly at a water flowrate of 1200 g/s.

4.3. Repeatability of the test series

The repeatability of the measurements was checked on the test series at Q_w = 1200 g/s with the rod bundle inserted into the test section. The mean and standard deviation values of the water mass flowrate and the air volume flowrate are similar in both test series and have a negligible impact on further measurements. Regarding the absolute pressure, a difference from 1 mbar to 5 mbar is noticed which leads to discrepancies up to 3 % of the void fraction (Cf. figure 6). The same trend is observed on the differential pressure curves with a difference up to 2 mbar from one test to the other that induces a variation on the void fraction up to 30 % (meaning 7 % void fraction absolute difference). These discrepancies put in light the intrinsic highly unstationary behavior of the hydraulics phenomena involved in the test section.

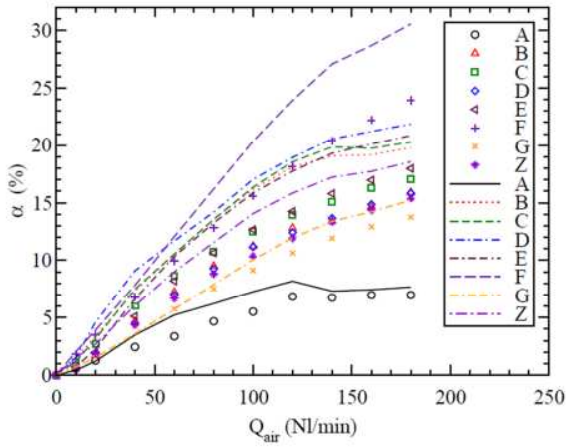

Figure 6. Comparison of the void fraction for the two tests series at a water flowrate of 1200 g/s (repeatability).

4.4. Analysis of the whole test series

Overall, the two-phase flows simulated during the tests exhibited two differing behaviors, depending on the investigated geometrical configuration. Those behaviors are discussed below.

First of all, with no rod bundle in the test section, the two-phase flows always correspond to a bubbly flow, with no noticeable bubble coalescence along the vertical axis. In this configuration, any increase of the gas superficial velocity leads to a gentle variation of the void fraction in the duct, as seen in figure 7b. At low gas superficial velocity, one may note that no clear trend can be observed when the liquid superficial velocity is varied. Visually, the flow exhibits a high level of randomness with bubbles fluctuating in all directions, in spite of their upward net movement.

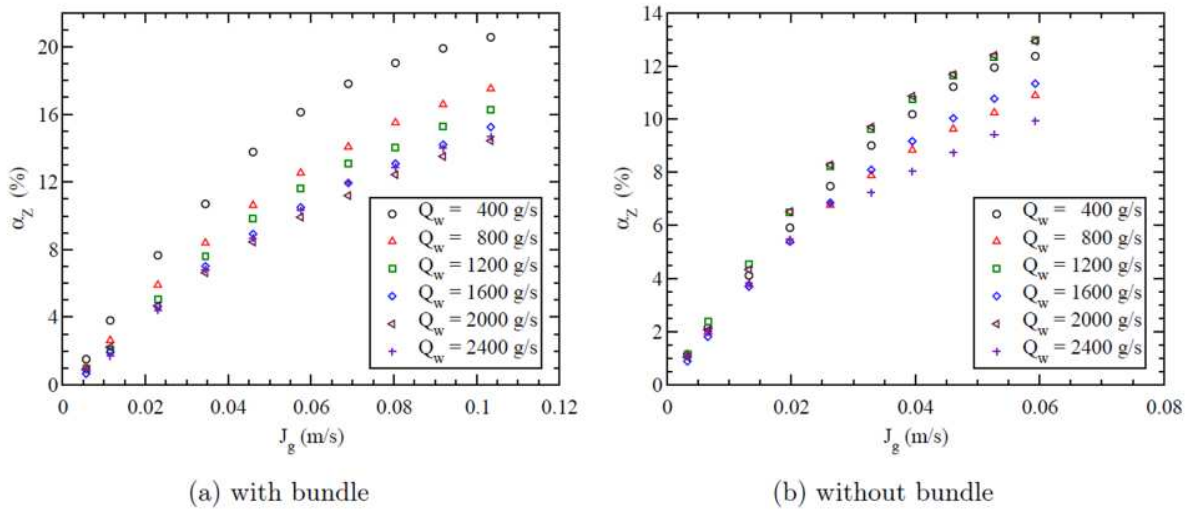

Figure 7. Mean void fraction over vertical direction as a function of the gas superficial velocity (J_g).

The two-phase flows within a rod bundle exhibit a different behavior. In such a case, a bubbly flow is first visualized for the gas superficial velocities lower than 5 cm/s. When more gas is added to the test section, the flow organizes differently and a cap-bubbly flow is reached, in which big gas pockets can be identified. The latter results from the coalescence of individual bubbles, promoted by the confinement imposed to the flow by the presence of the rod bundle. From that point, some big gas pockets accumulate sometimes below the rod bundle upper tie plate, thereby leading to macro-scale flow recirculations. Those recirculations are evidenced by tiny bubbles flowing downwardly and counter-currently to the main flow direction. As seen in figure 7a, an increase of the gas superficial velocity also leads to bigger void fractions. But, contrarily to the case with no bundle, a clear trend is observed here regarding changes in liquid superficial velocities: when more liquid is added to the test section, the void fraction reduces accordingly. Noticeably, for high liquid superficial velocities, this latter trend yields void fractions very close to the ones obtained with no rod bundle. We assume that an increasing liquid superficial velocity promotes bubbles dispersal by turbulent mixing within the test section and prevents big gas pockets formation and accumulation below the upper tie plate: qualitative flow observations show that those pockets are hardly visible in the test section at higher liquid superficial velocities.

5. CONCLUSIONS

One objective of the DENOPI project is to improve our understanding of the physical phenomena involved at the fuel assembly scale in a spent fuel pool in case of loss of cooling or loss of coolant accidents. The MEDEA-overflow experiments consist in a co-current air/water flow through a one meter height unheated rod bundle inserted into a SFP rack. In these experiments, no clear impact of the mixing grids and support grids on the void fraction profiles could be evidenced. Besides, two flow regimes were put in light. At low gas superficial velocities, a bubbly flow set up within the bundle whereas a transition to slug flow was observed at larger velocities. This experimental data will be considered in the near future to improve the modeling of this kind of flow by system codes especially by determining the most adequate drift flux model to recommend. Furthermore, the ASPIC facility, a heated full height assembly currently under construction, will enable in the near future several kinds of experiments and scenarios for SFP accidents at the assembly scale. For instance, boil-off scenarios will be considered with the evaluation of the efficiency of a water spray to cool down a partially/totally dry fuel bundle. Besides, measures of the pressure loss and void fraction along the assembly will be undertaken with a steam/water flow and compared to the results of the present study.

NOMENCLATURE

J_g	superficial gas velocity (m/s)
dP_A	pressure difference of the differential pressure transducer at location A (Pa)
P_{do}	pressure of the absolute pressure transducer at location do (Pa)
Q_w	water mass flowrate (kg/s)
Q_{air}	air volume flowrate (Nl/min)
α_A	void fraction at location A (-)
ρ_w	water volumetric mass density (kg/m^3)

ACKNOWLEDGMENTS

The DENOPI project is part of the "Investment for the future" program funded by the French Government within the framework of the post-Fukushima surveys identified as major safety issues (contract number ANR 11 - RSNR 006).

REFERENCES

1. D. Wang, I. C. Gauld, G. L. Yoder, L. J. Ott, G. F. Flanagan, M. W. Francis, E. L. Popov, J. J. Carbajo, P. K. Jain, J. C. Wagner, and J. C. Gehin, "Study of Fukushima Daiichi nuclear power station unit 4 spent-fuel pool," *Nucl. Tech.*, **180**(2), pp. 205-215 (2012).
2. X. Wu, W. Li, Y. Zhang, W. Tian, G. Su, and S. Qiu. "Analysis of accidental loss of pool coolant due to leakage in a PWR SFP," *Ann. Nucl. Energy*, **77**, pp. 65-73 (2015).
3. Y.-S. Chen and Y.-R. Yuann, "Accident mitigation for spent fuel storage in the upper pool of a Mark III containment," *Ann. Nucl. Energy*, **91**, pp. 156-164 (2016).
4. J.H. Song and T.W. Kim, "Severe accident issues raised by the Fukushima accident and improvements suggested," *Nucl. Eng. Tech.*, **46**(2), pp. 207-216 (2014).
5. Status report on spent fuel pools under loss-of-cooling and loss-of-coolant accident conditions. Technical Report NEA/OCDE 2015-2, Nuclear Energy Agency OCDE (2015).
6. O. Coindreau, B. Jäckel, F. Rocchi, F. Alcaro, D. Angelova, and G. Bandini, "Severe accident code-to-code comparison for two accident scenarios in a spent fuel pool". In of the 8th European Review Meeting on Severe Accident Research - ERMSAR (2017).
7. PIRT: R&D priorities for loss-of-cooling and loss-of-coolant accidents in spent nuclear fuel pools. Technical Report NEA/OCDE 2017-18, Nuclear Energy Agency OCDE (2017).
8. H. Mutelle, I. Tamburini, C. Duriez, S. Tillard, N. Trégourès, A. Toutant, V. Mermoux, V. Peres, and H. Buscail, "A new research program on accidents in spent fuel pools: the DENOPI project", Proceedings of WRFPM, Sensai, Japan, number 100071 (2014).
9. J. Martin, "Overview of the IRSN DENOPI project on spent fuel pool in loss-of-cooling and loss-of-coolant accident conditions," In CSARP, Bethesda, Maryland, USA, 2016.
10. J. Martin, G. Brillant, C. Duriez, N. Trégourès, and C. Marquié, "The IRSN DENOPI project: a research program on spent-fuel-pool loss-of-cooling and loss-of-coolant accidents" Proceedings of NURETH, Xi'an, China, 20745 (2017).
11. N. Trégourès, "The DENOPI project: a research program on SFP under loss-of-cooling and loss-of-coolant accident conditions," In IE8M, IAEA (2015).
12. H.-M. Prasser, A. Böttger, and J. Zschau, "A new electrode-mesh tomograph for gas-liquid flows," *Flow Meas. Instrum.*, **9**(2), pp. 111-119 (1998).
13. E. Schleicher, T.B. Aydin, R.E. Vieira, C.F. Torres, E. Pereyra, C. Sarica, and U. Hampel, "Refined reconstruction of liquid-gas interface structures for stratified two-phase flow using wire-mesh sensor," *Flow Meas. Instrum.*, **46**, pp. 230–239 (2015).